

# Reduced models for wave-balanced flow interactions

André Palóczy

January 19, 2022 (revised version)

## 1 Introduction and goals

Energy pathways in the ocean encompass the full range of scales from planetary,  $O(10^7 \text{ m})$  down to microscales,  $O(10^{-2} \text{ m})$ . Energy is introduced in the ocean mostly at seasonal, planetary scales by the time-mean atmospheric forcing; at diurnal, planetary scales by the most energetic modes of the barotropic tide; and in the weather band (days to weeks) by the synoptic weather systems. This energy must either leave the ocean or be converted into internal energy at the Kolmogorov scale,  $O(1 \text{ cm})$  [3].

The routes mechanical energy takes from injection to dissipation in the ocean are currently an open problem. A group of candidates that has been gaining attention over the past decade includes processes involving the interaction of near-inertial waves (NIWs) with the mesoscale balanced flow, *e.g.*, [14, 13, 7]. Two broad classes of such processes can be identified: The first is generation of NIWs by mesoscale and submesoscale instabilities, oftentimes called *spontaneous* loss of balance. The second is the interaction of the balanced flow with existing NIWs by processes such as refraction, advection and dispersion, a mechanism that has been more studied in recent years and has been called *stimulated* loss of balance, *e.g.*, [7].

The goals of this project are to: **1)** Study the energy exchanges between NIWs and the balanced flow using idealized simulations and **2)** To derive a new asymptotic model to help develop an understanding of such interactions.

## 2 Non-asymptotic reduced models

### 2.1 The modified Thomas & Yamada (2019) model

We develop a new reduced model consisting of the barotropic mode and a high baroclinic mode, which we denote as T-W model hereafter (Section 2.2 below). This model is a further reduction of the models implemented by [11] and [9]. We begin by generally following [11]’s derivation of the parent model to the T-W model. The starting point is the hydrostatic Boussinesq equations, with the assumption of constant buoyancy frequency  $N$ :

$$\mathbf{u}_t + \mathbf{u} \cdot \nabla \mathbf{u} + w \mathbf{u}_z + \mathbf{f} \times \mathbf{u} + \nabla p = 0, \quad (1)$$

$$p_z = b, \quad (2)$$

$$b_t + \mathbf{u} \cdot \nabla b + w N^2 = 0, \quad (3)$$

$$\nabla \cdot \mathbf{u} + w_z = 0, \quad (4)$$

where  $(u, v, w)$  are the velocity components of  $\mathbf{u}$  in the  $(\hat{\mathbf{x}}, \hat{\mathbf{y}}, \hat{\mathbf{z}})$  directions, respectively,  $p$  is pressure (normalized by a reference density  $\rho_0$ ),  $b \equiv -g\rho'/\rho_0$  is the buoyancy (where  $\rho'$  is the perturbation pressure),  $\nabla \equiv \hat{\mathbf{x}}\partial_x + \hat{\mathbf{y}}\partial_y$  is the horizontal gradient operator,  $\mathbf{f} \equiv \hat{\mathbf{z}}f$  (where  $f$  is the inertial frequency) and  $N$  is the buoyancy frequency. We expand all variables in the following form:

$$\mathbf{u}(\mathbf{x}, z, t) = \mathbf{u}_0(\mathbf{x}, t) + \sum_{n=1}^{\infty} \mathbf{u}(\mathbf{x}, t) \phi'_n(z) \quad (5)$$

$$w(\mathbf{x}, z, t) = \sum_{n=1}^{\infty} w(\mathbf{x}, t) \phi_n(z) \quad (6)$$

$$p(\mathbf{x}, z, t) = p_0(\mathbf{x}, t) + \sum_{n=1}^{\infty} \lambda_n^{-2} p_n(\mathbf{x}, t) \phi'_n(z) \quad (7)$$

$$b(\mathbf{x}, z, t) = - \sum_{n=1}^{\infty} p_n(\mathbf{x}, t) N^2 \phi_n(z) \quad (8)$$

where  $\phi_{n=0}(z) = 1$ ,  $\phi_{n>0} = \sin(n\pi z)$  is the solution of the Sturm-Liouville problem with constant stratification  $N(z) = 1$  and rigid lid boundary conditions, *i.e.*,

$$\phi_n'' + \lambda_n^2 N^2 \phi_n = 0, \quad \text{with} \quad \phi_n(0) = \phi_n(1) = 0 \quad (9)$$

where the eigenvalues are  $\lambda_{n=0} = 0$  and  $\lambda_{n>0} = n\pi$ .

Restricting 5-8 to the barotropic mode (subscript  $T$ ) and the  $n$ -th baroclinic mode (subscript  $C$ ) gives

$$\mathbf{u}(\mathbf{x}, t), p(\mathbf{x}, t) = [\mathbf{u}_T(\mathbf{x}, t), p_T(\mathbf{x}, t)] + [\mathbf{u}_C(\mathbf{x}, t), p_C(\mathbf{x}, t)] \times \sqrt{2} \cos\left(\frac{n\pi z}{H}\right) \quad (10)$$

$$w(\mathbf{x}, t), b(\mathbf{x}, t) = [w_C(\mathbf{x}, t), b_C(\mathbf{x}, t)] \times \sqrt{2} \sin\left(\frac{n\pi z}{H}\right), \quad (11)$$

Substituting 10-11 into 1-4 and using the orthogonality property of the modes results in equations similar to the linear shallow water equations for the  $n$ -th baroclinic mode ( $n \geq 1$ ):

$$\partial_t \mathbf{u}_T + \mathbf{f} \times \mathbf{u}_T + \nabla p_T + \text{Ro}[\mathbf{u}_T \cdot \nabla \mathbf{u}_T + \mathbf{u}_C \cdot \nabla \mathbf{u}_C + (\nabla \cdot \mathbf{u}_C) \mathbf{u}_C] = 0, \quad (12)$$

$$\nabla \cdot \mathbf{u}_T = 0, \quad (13)$$

$$\partial_t \mathbf{u}_C + \mathbf{f} \times \mathbf{u}_C + \nabla p_C + \text{Ro}(\mathbf{u}_T \cdot \nabla \mathbf{u}_C + \mathbf{u}_C \cdot \nabla \mathbf{u}_T) = 0, \quad (14)$$

$$\partial_t p_C + \left(\frac{NH}{n\pi}\right)^2 \nabla \cdot \mathbf{u}_C + \text{Ro}(\mathbf{u}_T \cdot \nabla p_C) = 0, \quad (15)$$

where the Rossby number is (with characteristic velocity and horizontal length scales  $U$  and  $L$ , respectively)

$$\text{Ro} \equiv \frac{U}{fL}. \quad (16)$$

Taking curl of the T-mode's momentum equation 12 to eliminate  $p_T$ ,

$$\partial_t \zeta_T + \text{Ro} \nabla \times [\mathbf{u}_T \cdot \nabla \mathbf{u}_T + \mathbf{u}_C \cdot \nabla \mathbf{u}_C + (\nabla \cdot \mathbf{u}_C) \mathbf{u}_C] = 0, \quad (17)$$

where  $\zeta_T \equiv \partial_x v_T - \partial_y u_T$ . Rescaling the baroclinic pressure as  $p_C \rightarrow \text{Bu}_n p_C$  gives the final set of equations:

$$\partial_t \zeta_T + \text{Ro} \nabla \times [\mathbf{u}_T \cdot \nabla \mathbf{u}_T + \mathbf{u}_C \cdot \nabla \mathbf{u}_C + (\nabla \cdot \mathbf{u}_C) \mathbf{u}_C] = 0, \quad (18)$$

$$\partial_t \mathbf{u}_C + \hat{\mathbf{z}} \times \mathbf{u}_C + \text{Bu}_n \nabla p_C + \text{Ro}(\mathbf{u}_T \cdot \nabla \mathbf{u}_C + \mathbf{u}_C \cdot \nabla \mathbf{u}_T) = 0, \quad (19)$$

$$\partial_t p_C + \nabla \cdot \mathbf{u}_C + \text{Ro}(\mathbf{u}_T \cdot \nabla p_C) = 0, \quad (20)$$

where the modal Burger number is (with a characteristic vertical length scale  $H$ )

$$\text{Bu}_n \equiv \left(\frac{NH}{\lambda_n f L}\right)^2 \quad (21)$$

where the baroclinic mode is a high mode, rather than the first baroclinic mode considered by [11].

Two-dimensional models obtained from truncating three-dimensional equations to few modes have been used elsewhere in the literature, *e.g.*, [4, 2]. We call this the modified Thomas & Yamada (2019) model because [11] treated only the particular case where  $\text{Bu} = 1$ , relevant to the first mode of the internal tide rather than near-inertial waves. This difference can be seen by considering the nondimensional dispersion relation for inertia-gravity waves:

$$\omega^2 = f^2(1 + \text{Bu}_w), \quad (22)$$

where  $\omega$  is the wave frequency,  $\text{Bu}_w \equiv [Nk_h/(fk_z)]^2$  is the wave Burger number,  $k_h \equiv \sqrt{k_x^2 + k_y^2}$  is the magnitude of the horizontal wavenumber vector and  $k_z$  is the vertical

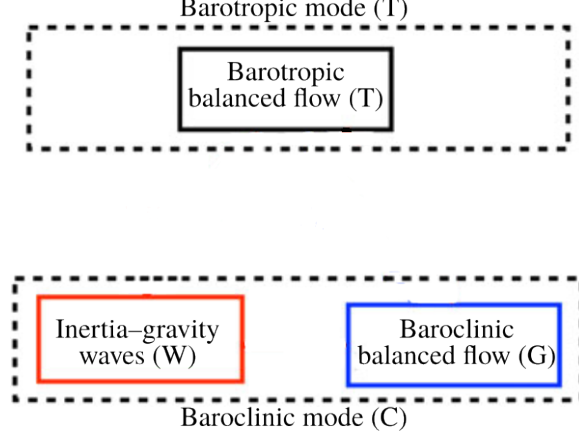


Figure 1: Schematic showing the three components of the modified Thomas & Yamada (2019) model: The barotropic mode ( $T$ -mode) consists only of purely geostrophically-balanced flow, while the baroclinic mode consists of geostrophically-balanced flow ( $G$ -mode) and unbalanced (near-inertial) wave motions ( $W$ -mode).

component of the wavenumber vector. Since near-inertial waves have more energy content in high baroclinic modes,  $\omega \approx f$ , due to which  $\text{Bu}_w \ll 1$ . This is the limit considered in this project. The dynamical components of the system described by 18-20 are represented schematically in Figure 1. The barotropic mode ( $T$ -mode) contains only geostrophically-balanced energy, while the baroclinic mode contains both balanced energy ( $G$ -mode) and unbalanced inertia-gravity wave energy.

In order to further specialize the model to study the interactions between near-inertial waves and balanced flows, we suppress the  $G$ -mode at every time step by inverting the linear baroclinic potential vorticity  $q \equiv \zeta_C - p_C = \zeta_G - p_G$  and subtracting out the balanced velocity from the total baroclinic velocity vector  $\mathbf{u}_C$ . This is possible because only the balanced flow projects on  $q$ , since near-inertial waves have no linear potential vorticity.

## 2.2 The coupled T-W model

A more elegant and less artificial approach to isolate interactions between near-inertial waves and a balanced barotropic flow is to seek a simpler, two-component model (Figure 2) where the prognostic variables are pure wave quantities. We start from the equations of motion (with the  $C$  subscript dropped):

$$\partial_t \mathbf{u}_T + \hat{\mathbf{z}} \times \mathbf{u}_T + \nabla p_T = \mathbf{F}_T^u, \quad (23)$$

$$\partial_t \mathbf{u} + \hat{\mathbf{z}} \times \mathbf{u} + \text{Bu} \nabla p = \mathbf{F}^u, \quad (24)$$

$$\partial_t p + \nabla \cdot \mathbf{u} = \mathbf{F}^p, \quad (25)$$

where  $\mathbf{u}$  and  $\mathbf{u}_T$  are respectively the baroclinic wavy and barotropic geostrophically balanced velocities and

$$\mathbf{F}_T^u \equiv -\text{Ro}[\mathbf{u}_T \cdot \nabla \mathbf{u}_T + \mathbf{u} \cdot \nabla \mathbf{u} + (\nabla \cdot \mathbf{u})\mathbf{u}], \quad (26)$$

$$\mathbf{F}^u \equiv -\text{Ro}(\mathbf{u}_T \cdot \nabla \mathbf{u} + \mathbf{u} \cdot \nabla \mathbf{u}_T), \quad (27)$$

$$\mathbf{F}^p \equiv -\text{Ro}(\mathbf{u}_T \cdot \nabla p) \quad (28)$$

We can define a velocity potential  $\phi$  and a streamfunction  $\chi$  such that

$$u = \phi_x - \chi_y, \quad (29)$$

$$v = \phi_y + \chi_x, \quad (30)$$

$$u + iv = \underbrace{(\partial_x + i\partial_y)}_{\equiv \partial_s} \underbrace{(\phi + i\chi)}_{\equiv A}, \quad (31)$$

and

$$\phi = \phi_W, \quad (32)$$

$$\chi = \chi_G + \chi_W, \quad (33)$$

$$p = p_G + p_W, \quad (34)$$

$$(35)$$

where the subscripts  $G$  and  $W$  indicate baroclinic balanced (G-mode in Figure 1) and wave (W-mode in Figure 1) quantities, respectively. The G-mode satisfies

$$\hat{\mathbf{z}} \times \mathbf{u}_G + \text{Bu} \nabla p_G = 0, \quad (36)$$

$$\nabla \cdot \mathbf{u}_G = 0, \quad (37)$$

while the W-mode satisfies

$$\partial_t \mathbf{u}_W + \hat{\mathbf{z}} \times \mathbf{u}_W + \text{Bu} \nabla p_W = 0, \quad (38)$$

$$\partial_t p_W + \nabla \cdot \mathbf{u}_W = 0. \quad (39)$$

Defining the Laplacian operator  $\Delta \equiv \partial_x^2 + \partial_y^2$  and taking  $\nabla \cdot 36$ , we have

$$-\zeta_G + \text{Bu} \Delta p_G = 0 \Rightarrow \text{Bu} \Delta p_G - \Delta \chi_G = 0 \Rightarrow \chi_G = \text{Bu} p_G. \quad (40)$$

We form a conservation statement for the linear potential vorticity by setting  $\text{Ro} = 0$  in 23, 24 and 25 and taking  $\nabla \times 24 - 25$ , defining  $\zeta = \nabla \times \mathbf{u}$ :

$$\partial_t(\zeta - p) = 0 \Rightarrow \partial_t(\zeta_G - p_G) + \partial_t(\zeta_W - p_W) = 0. \quad (41)$$

at this point we note that in the present model, inertia-gravity waves have no linear potential vorticity, and therefore the combination  $\zeta_W - p_W$  is identically zero. This implies

$$p_W = \zeta_W \Rightarrow p_W = \Delta\chi_W. \quad (42)$$

Back to 41, we have

$$\partial_t(\underbrace{\zeta_G - p_G}_{\equiv q_G}) = 0. \quad (43)$$

If we now make the choice  $q_G = 0$  at  $t = 0$ , it follows that

$$p_G = \zeta_G \Rightarrow p_G = \Delta\chi_G. \quad (44)$$

Using 40 in 44, it follows that

$$p_G = \text{Bu}\Delta p_G. \quad (45)$$

The only way that 45 can be satisfied is if  $p_G = 0$  for all  $t$ , from which it follows that  $\chi_G = 0$ ,  $p = p_W$  and  $\chi = \chi_W$ . The choice of zero baroclinic potential vorticity  $q_G$  thus eliminates the G-mode, resulting in the two-component system represented in Figure 2.

The next step is to obtain evolution equations for  $\phi$  and  $\chi$ . Taking  $\nabla \cdot 24$ ,  $\nabla \times 24$  and  $\Delta 25$  yields, respectively,

$$\partial_t(\underbrace{\nabla \cdot \mathbf{u}}_{\Delta\phi}) - \Delta\chi + \text{Bu}\Delta p = \nabla \cdot \mathbf{F}^u, \quad (46)$$

$$\partial_t(\underbrace{\nabla \times \mathbf{u}}_{\Delta\chi}) + \Delta\phi = \nabla \times \mathbf{F}^u, \quad (47)$$

$$\partial_t(\Delta p) + \Delta^2\phi = \Delta \mathbf{F}^p. \quad (48)$$

Taking 47 - Bu $\times$ 48,

$$\partial_t\Delta(\chi - \text{Bu}p) = -\Delta(1 - \text{Bu}\Delta)\phi + \nabla \times \mathbf{F}^u - \text{Bu}\Delta \mathbf{F}^p. \quad (49)$$

We then note that

$$\chi - \text{Bu}p = \underbrace{\chi_G - \text{Bu}p_G}_{=0} + \chi_W - \text{Bu}p_W = \chi_W - \text{Bu}p_W, \quad (50)$$

where the last equality in 50 follows from 40. Using 42 in 49:

$$\partial_t \Delta(\chi - \text{Bu} \Delta \chi) = -\Delta(1 - \text{Bu} \Delta) \phi + \nabla \times \mathbf{F}^u - \text{Bu} \Delta \mathbf{F}^p. \quad (51)$$

or

$$\boxed{\partial_t \chi = \Delta^{-1} (1 - \text{Bu} \Delta)^{-1} \nabla \times \mathbf{F}^u - \text{Bu} (1 - \text{Bu} \Delta)^{-1} \mathbf{F}^p - \phi.} \quad (52)$$

By using 42 in 46, we obtain

$$\partial_t (\Delta \phi) = \Delta(1 - \text{Bu} \Delta) \chi + \nabla \cdot \mathbf{F}^u, \quad (53)$$

or

$$\boxed{\partial_t \phi = (1 - \text{Bu} \Delta) \chi + \Delta^{-1} (\nabla \cdot \mathbf{F}^u).} \quad (54)$$

Taking  $\nabla \times 23$  and noting that  $\nabla \cdot \mathbf{u}_T = 0$  gives the evolution equation for the T-mode's vorticity  $\zeta_T = \Delta \Psi$ , where  $\Psi$  is the T-mode's streamfunction:

$$\boxed{\partial_t \zeta_T = \nabla \times \mathbf{F}_T^u.} \quad (55)$$

We now seek an evolution equation for the purely inertial wave mode (the zeroth wavenumber wave). This mode's velocity is spatially uniform across the domain, and therefore can be isolated by taking the spatial average (denoted by  $\langle \bullet \rangle$ ) of the momentum equation 24:

$$\langle \mathbf{u}_t \rangle + \hat{\mathbf{z}} \times \langle \mathbf{u} \rangle + \langle \text{Bu} \nabla p \rangle = \langle \mathbf{F}^u \rangle \quad (56)$$

Defining  $A_0 \equiv \langle u \rangle + i \langle v \rangle = u_0 + i v_0$ , the  $\hat{\mathbf{x}}$  and  $\hat{\mathbf{y}}$  components of 56 are, respectively,

$$\partial_t u_0 - v_0 = \Re \langle \mathbf{F}^u \rangle, \quad (57)$$

$$\partial_t v_0 + u_0 = \Im \langle \mathbf{F}^u \rangle \quad (58)$$

Taking 57 +  $i \times$  58 yields

$$\boxed{\partial_t A_0 = -i A_0 + \Re \langle \mathbf{F}^u \rangle + i \Im \langle \mathbf{F}^u \rangle.} \quad (59)$$

Equations 52, 54, 55 and 59 form a set of evolution equations for the barotropic vorticity  $\zeta_T$  (T-mode), the near-inertial wave amplitude  $A \equiv \phi + i \chi$  (W-mode) and the pure inertial oscillation's amplitude  $A_0$ .

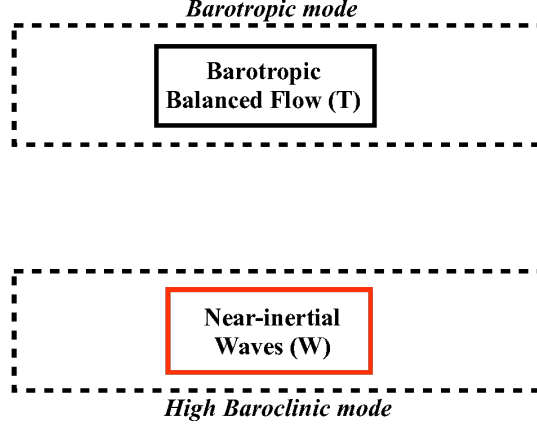


Figure 2: Schematic showing the two components of the  $T-W$  model: The barotropic mode ( $T$ -mode) consists only of purely geostrophically-balanced flow, while the high baroclinic mode consists only of unbalanced (near-inertial) wave motions.

### 2.2.1 Energetics of the coupled T-W model

We may obtain equations for the kinetic energy of the divergent and rotational parts of the wave velocity by taking  $\phi \times 53$  and  $\chi \times \Delta 52$ , respectively, and integrating over the domain. The result is (recalling from 42 that  $p = \Delta\chi$ ),

$$\frac{\partial}{\partial t} \frac{1}{2} \langle |\nabla\phi|^2 \rangle = \langle \nabla\phi \cdot \nabla\chi \rangle - \text{Bu} \langle \nabla\phi \cdot \nabla(\Delta\chi) \rangle + \langle \mathbf{F}^u \cdot \nabla\phi \rangle, \quad (60)$$

and

$$\frac{\partial}{\partial t} \frac{1}{2} \langle |\nabla\chi|^2 \rangle = -\langle \nabla\phi \cdot \nabla\chi \rangle - \langle \chi(1 - \text{Bu}\Delta)^{-1} (\nabla \times \mathbf{F}^u - \text{Bu}\Delta \mathbf{F}^p) \rangle. \quad (61)$$

The first term on the right-hand sides of 60 and 61 appears with opposite signs in both equations and can therefore be interpreted as a conversion term that represents the kinetic energy transfers between the rotational and divergent parts of the wave field.

Recalling again that  $p = \Delta\chi$ , we can also form a potential energy equation by taking  $\Delta\chi \times \Delta 52$  and integrating over the domain to obtain

$$\frac{\partial}{\partial t} \frac{1}{2} \langle (\Delta\chi)^2 \rangle = -\langle \Delta\chi \Delta\phi \rangle + \langle \Delta\chi(1 - \text{Bu}\Delta)^{-1} (\nabla \times \mathbf{F}^u - \text{Bu}\Delta \mathbf{F}^p) \rangle. \quad (62)$$

The pure inertial mode's energy equation can be obtained by taking  $A_0^* \times 59$ , adding the entire expression's complex conjugate and dividing the result by two (where the star superscript indicates the complex conjugate):

$$\frac{\partial}{\partial t} \frac{1}{2} |A_0|^2 = \Re \langle \mathbf{F}^u \rangle \Re A_0 + \Im \langle \mathbf{F}^u \rangle \Im A_0. \quad (63)$$

Finally, the T-mode's energy equation can be obtained by taking  $-\Psi \times 55$  and integrating over the domain.

$$\partial_t \frac{1}{2} \langle \Psi \zeta_T \rangle = \langle \Psi \nabla \times \mathbf{F}_T^u \rangle. \quad (64)$$

It can be verified numerically that the system conserves total energy, that is, (60) + (61) + Bu × (62) + (63) + (64) = 0:

$$\frac{\partial}{\partial t} \frac{1}{2} \iint |\nabla \phi|^2 + |\nabla \chi|^2 + \text{Bu}(\Delta \chi)^2 + |A_0|^2 - \Psi \zeta_T dA = 0. \quad (65)$$

### 3 Parameter sweep with the linearized modified Thomas & Yamada (2019) model

Next, we explore the sensitivity of the energy changes to different barotropic flows in the linearized version of 18-20 (linearized about a steady barotropic balanced flow  $\mathbf{U} = \hat{\mathbf{x}}U + \hat{\mathbf{y}}V$ ). We solve 18-20 using a standard pseudo-spectral code based on [10]. Figure 3 compares the evolution of wave kinetic, potential and total energies for simulations with barotropic balanced flows with randomized phase and increasing number of initial wavenumbers  $K_i$ .

The wave amplitude can be further approximately decomposed into clockwise and counter-clockwise motions as follows:

$$\mathcal{U} = A^- e^{-it} + A^+ e^{it} \quad (66)$$

So that the kinetic energy is

$$\frac{1}{2} \iint \overline{\mathcal{U}} \mathcal{U} dx dy = \frac{1}{2} \iint |A^-|^2 + |A^+|^2 + \overline{A^-} A^+ e^{+2it} + \overline{A^+} A^- e^{-2it} dx dy \quad (67)$$

and the potential energy is (using the fact that  $p^+ = \overline{p^-}$ )

$$\frac{1}{2} \iint \overline{p} p dx dy = \frac{1}{2} \iint 2|p^-|^2 + \overline{p^-} \overline{p^-} e^{+2it} + p^- p^- e^{-2it} dx dy \quad (68)$$

Figure 4 compares the evolution of the wave energy terms associated with positive (proportional to  $A^+$ ) negative (proportional to  $A^-$ ) and mixed (proportional to  $\overline{A^+} A^- + \text{c.c.}$ ) amplitudes. It can be seen that the cross component has magnitude comparable to the + and - components, indicating that this decomposition is non-orthogonal, contrary to the orthogonal decompositions used in *e.g.*, [5, 11].

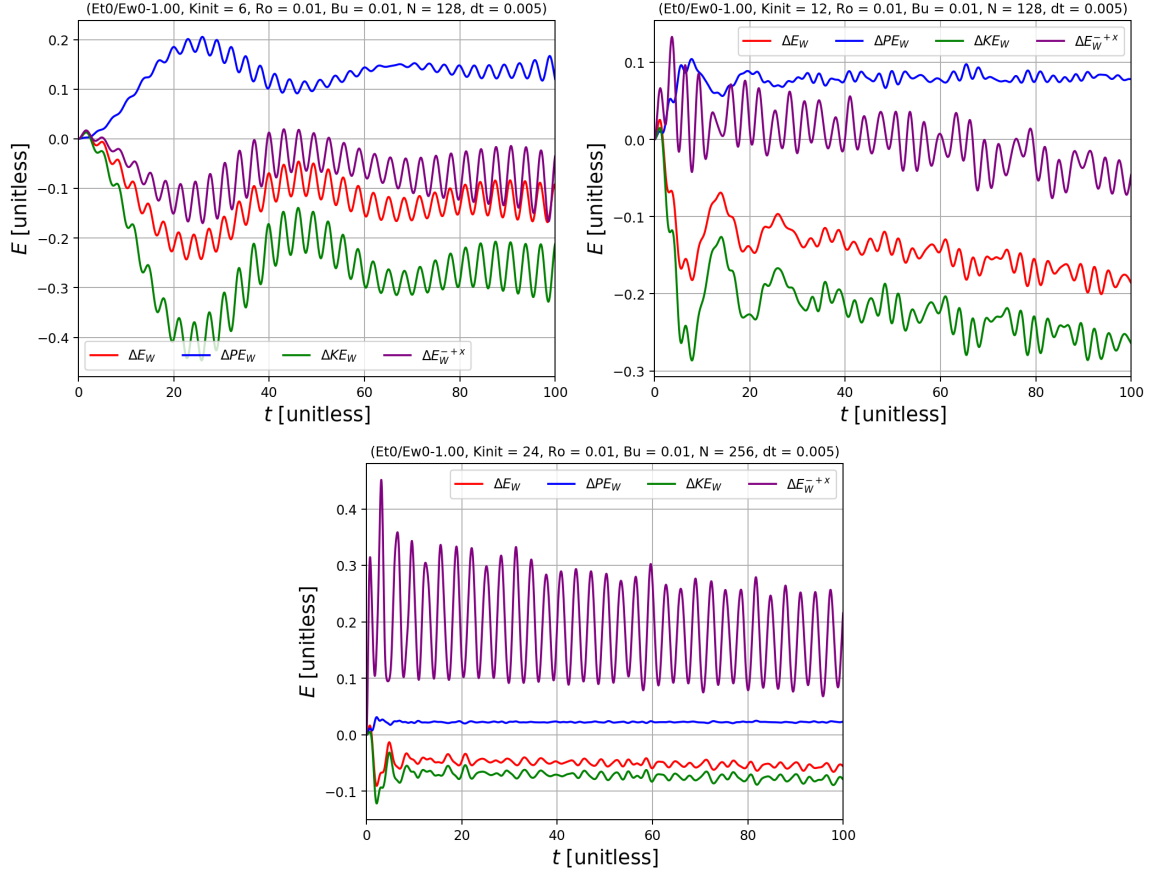


Figure 3: Wave energy changes for 6 (top left) 12 (top right) and 24 (bottom) initial wavenumbers in the system evolving according to Equations 18-20. Note that the wave potential energy gain is offset by the wave kinetic energy loss, causing the total wave energy to decrease.

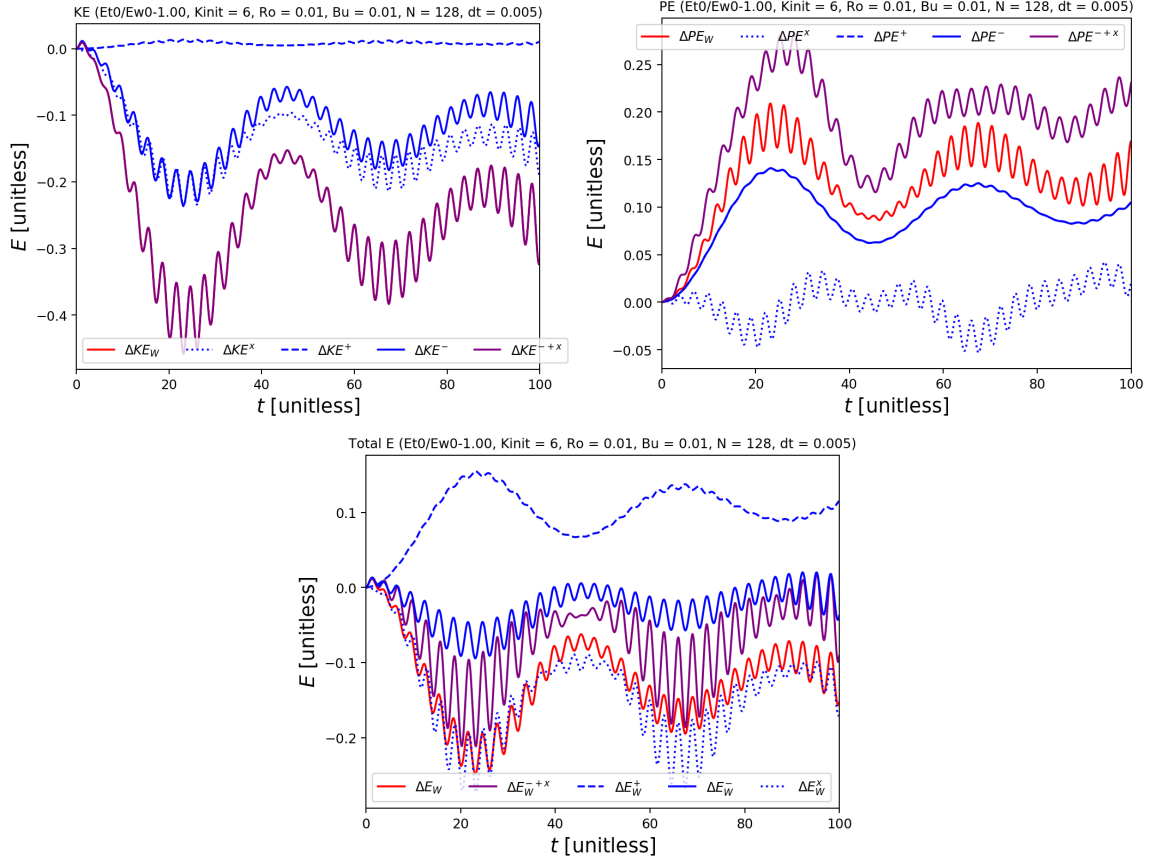


Figure 4: Kinetic (top left), potential (top right) and total (bottom) wave energy changes in the system evolving according to Equations 18-20 for the approximate decomposition in  $+$ ,  $-$  and  $x$  (cross) terms. Note that the cross terms are not negligible, indicating that this simplified decomposition is non-orthogonal.

## 4 Helmholtz decomposition of reduced model solutions

In this section we briefly compare the energy partitioning into rotational (balanced, non-divergent) and divergent (unbalanced, irrotational) motions in the linearized version of 18-20 with the partitioning in the simpler Young and Ben Jelloul (YBJ, [14]) model. The total velocity field can be decomposed into a velocity potential  $\phi$  (irrotational) and a streamfunction  $\psi$  (non-divergent) according to

$$\psi = \Delta^{-1}(v_x - u_y), \quad (69)$$

$$\phi = \Delta^{-1}(u_x + v_y), \quad (70)$$

$$u + iv = (\partial_x + i\partial_y)(\phi + i\psi). \quad (71)$$

Figure 5 shows the spatial distribution of the wave kinetic energy density in a simulation of the linearized 18-20 system. Figure 6 shows the energy evolution in different reservoirs, which is similar in both systems: The purely inertial mode (inertial oscillations evolving according to 59, dashed black lines) loses kinetic energy while the near-inertial modes gain kinetic energy. This energy gain is approximately equipartitioned between rotational and divergent motions. It can also be seen that the wave kinetic energy decreases in the linearized 18-20 solution, while it stays constant in the YBJ solution, as predicted by one of its conservation laws [14]. The fact that the YBJ system conserves wave kinetic energy is one of its limitations.

## 5 Wave-balanced flow interaction: Case studies

In this section we aim to gain some physical intuition on the wave-balanced flow interaction by analyzing a set of initial value problems with different barotropic flows as initial conditions. Specifically, we seek answers to the following questions:

1. How do different balanced flows couple with the near-inertial wave field?
2. what is the direction of the energy transfers, *i.e.*, from balanced flow to waves or from waves to balanced flow?

The system simulated is 18-20, where the barotropic flow evolves according to Equation 18 and therefore has a two-way coupling with the near-inertial waves. The balanced part of the baroclinic mode is removed by inverting the potential vorticity. Although the two-component  $T$ - $W$  model has not been numerically implemented yet, it is expected to give similar results.

We begin with an initial barotropic flow of a simple Gaussian anticyclone (Figure 7) in the presence of a spatially uniform inertial oscillation. As is well known in the literature (*e.g.*, [7]), wave kinetic energy density gets trapped inside anticyclonic vortices, as observed in this experiment (top-right panels in Figure 7). The total balanced energy increases at the expense of the total wave energy, and the skewness of the barotropic vorticity changes from negative to slightly positive by  $t = 200$  (bottom panel of Figure 7), indicating a change in the predominance of anticyclones (negative vorticity) to cyclones (positive vorticity).

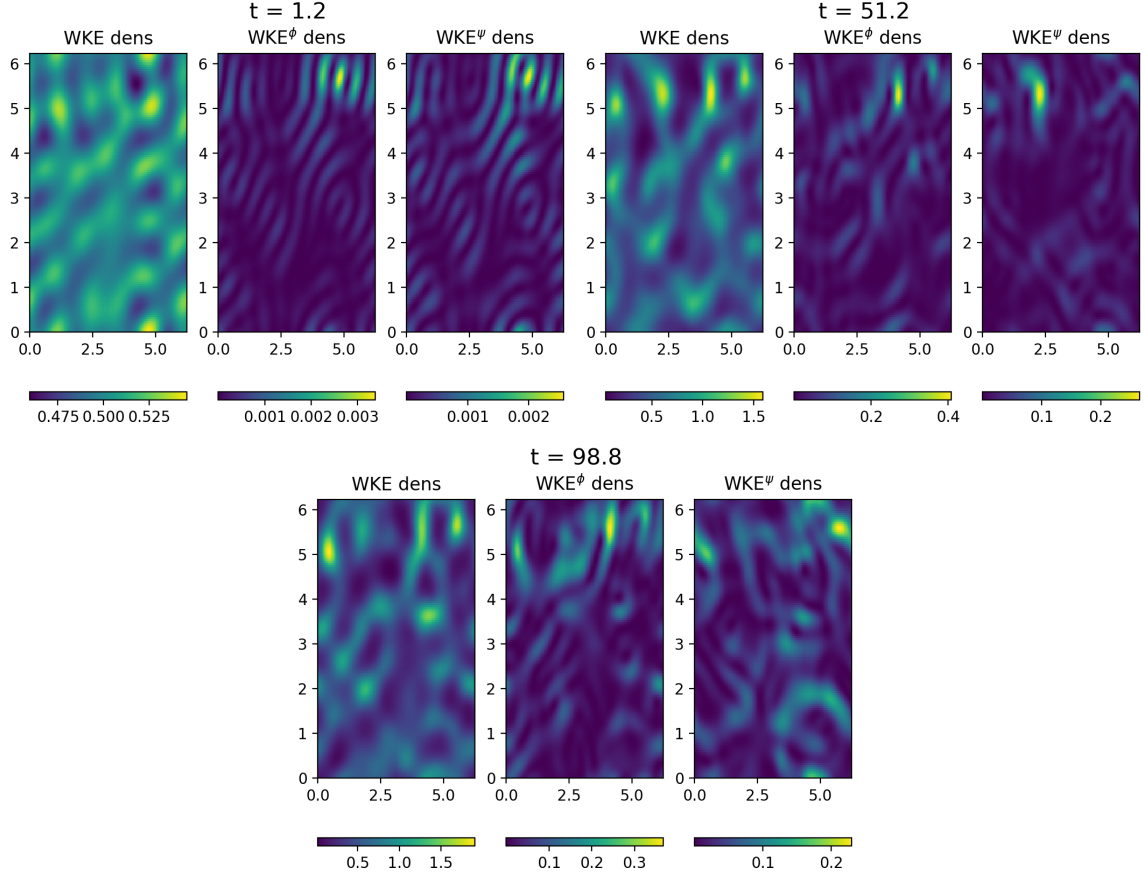


Figure 5: Kinetic energy density snapshots of a linearized 18-20 solution decomposed into rotational ( $\psi$ ) and divergent ( $\phi$ ) parts.

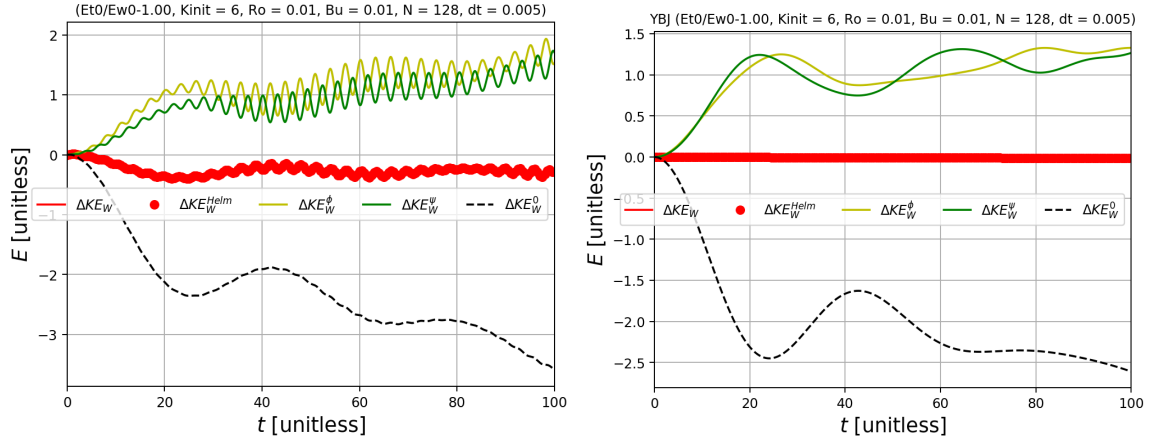


Figure 6: Energy changes for the linearized 18-20 system (left) and the YBJ system (right). The kinetic energy is decomposed into rotational ( $\psi$ , green) and divergent ( $\phi$ , yellow) parts.

When the initial barotropic flow is a cyclone superimposed on a spatially uniform inertial oscillation, wave kinetic energy density is repelled from the core of the vortex (top-right panels of Figure 8), contrary to the anticyclonic case described in the previous paragraph. The skewness changes from positive to negative, also in contrast with the anticyclonic case. However, the energy changes of the cyclonic case are qualitatively similar to the anticyclonic case (bottom panel of Figure 8).

Does this energy pathway change direction as  $\text{Ro} \rightarrow 1$ ? Figure 9 shows results of a simulation identical to that in Figure 7, except for the Rossby number, which is set to 1. Numerical instability sets in very early on in the simulation, and total energy is no longer conserved after  $t \approx 2.5$ . However, if not an initial transient or a numerical artifact, the behavior seen at  $t < 2.5$  could suggest that the energy exchange changes direction, with waves now extracting energy from the balanced flow. This would imply that it is possible to reproduce the behavior of fully three-dimensional, non-hydrostatic Boussinesq simulations at  $\text{Ro} \sim 1$  (e.g., [1]) with this simple two-dimensional model.

When the initial conditions have both anticyclones and cyclones randomly distributed across a few low wavenumbers, the behavior is qualitatively similar to when only one sign of vorticity is initially present, in the sense that anticyclones trap wave energy while cyclones repel it (upper-right panels of Figures 10 and 11). The energy changes are also similar, with the waves losing total energy while the balanced flow gains total energy. The wave energy is initially contained entirely in the purely inertial, spatially uniform mode ( $k = 0$ ), but it decreases rapidly mirroring the increase in wave energy in the higher modes ( $k \neq 0$ ). Importantly, the energy changes appear to be relatively insensitive to the relationship between  $\text{Ro}$  and  $\text{Bu}$  and the initial balanced/wave energy ratio,  $E_{t0}/E_{w0}$  (compare Figure 10, where  $\text{Bu} = \text{Ro} = 0.01$  and  $E_{t0}/E_{w0} = 1$ , with Figure 11, where  $\text{Bu} = \text{Ro}^2 = 0.01$  and  $E_{t0}/E_{w0} = 0.01$ ). The vortices in the simulation where  $E_{t0}/E_{w0} = 0.01$  are more deformed, with a less smooth vorticity distribution (compare upper-right panels of Figures 10 and 11), indicating that the balanced flow can be appreciably impacted by the near-inertial waves in this strong wave regime.

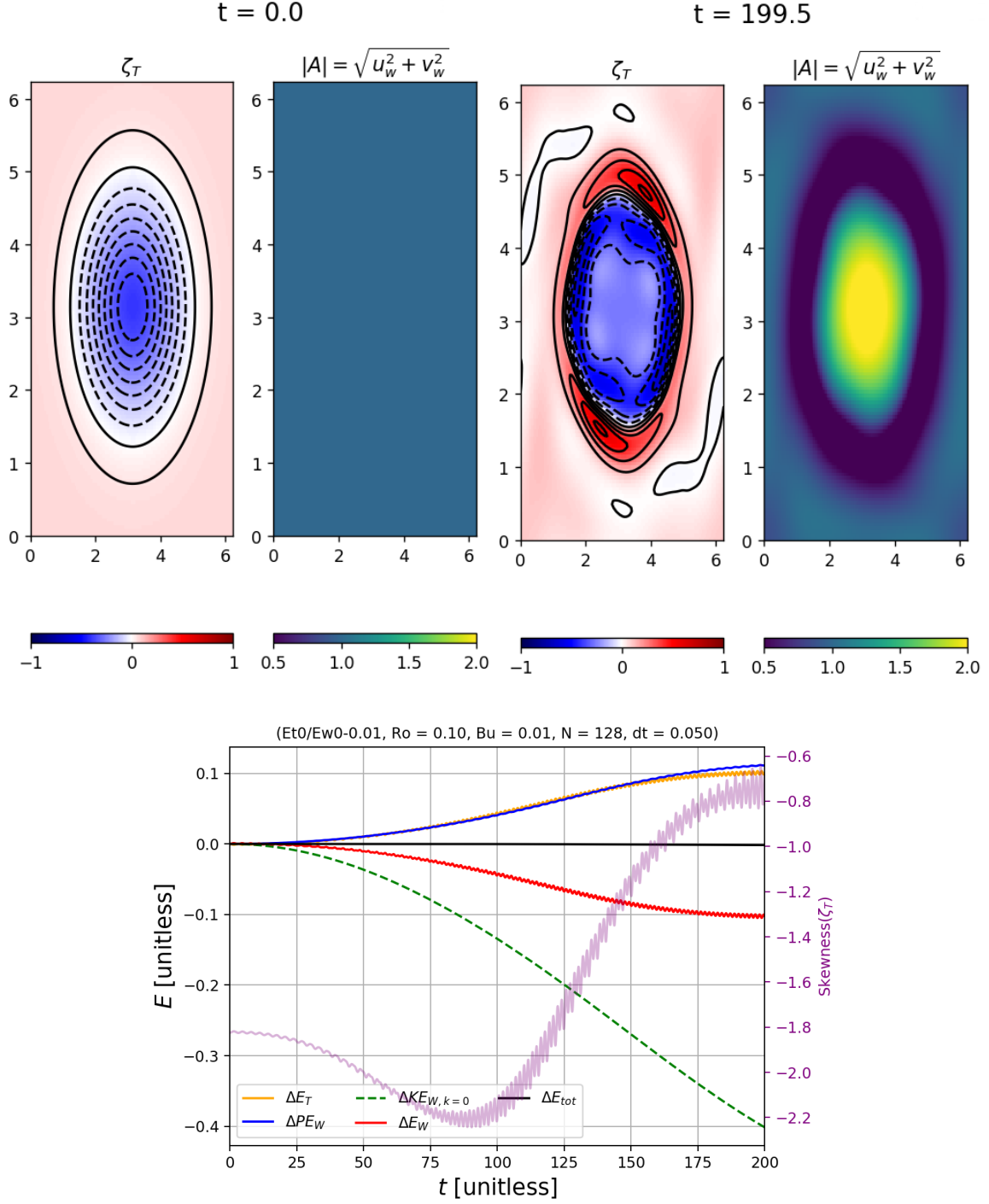


Figure 7: Coupled T-W wave energy changes (lower panel) and snapshots of the barotropic vorticity  $\zeta_T$  and the wave amplitude  $|A|$  (upper panels), initialized with a barotropic anti-cyclone.  $\Delta E_T$ ,  $\Delta E_{tot}$ ,  $\Delta PE_W$ ,  $\Delta KE_{W,k=0}$  and  $\Delta E_W$  are the balanced barotropic energy, the total (wave + balanced) energy, the wave potential energy, the wave kinetic energy in the purely inertial mode ( $k = 0$ ) and the total wave energy, respectively. The purple line in the lower panel is the instantaneous skewness of the barotropic vorticity.  $E_{t0}/E_{w0}$  is the initial balanced-to-wave energy ratio, and  $N$  and  $dt$  are respectively the number of Fourier modes and the time step in the simulation. 15

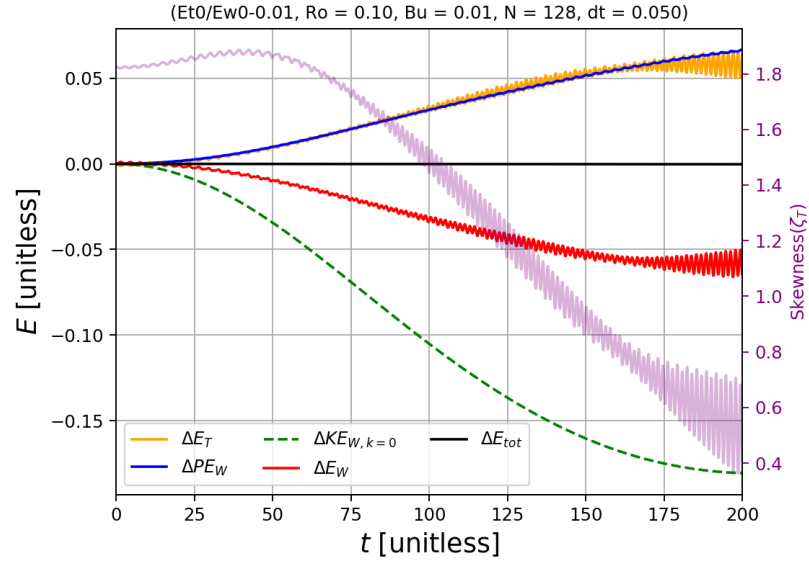
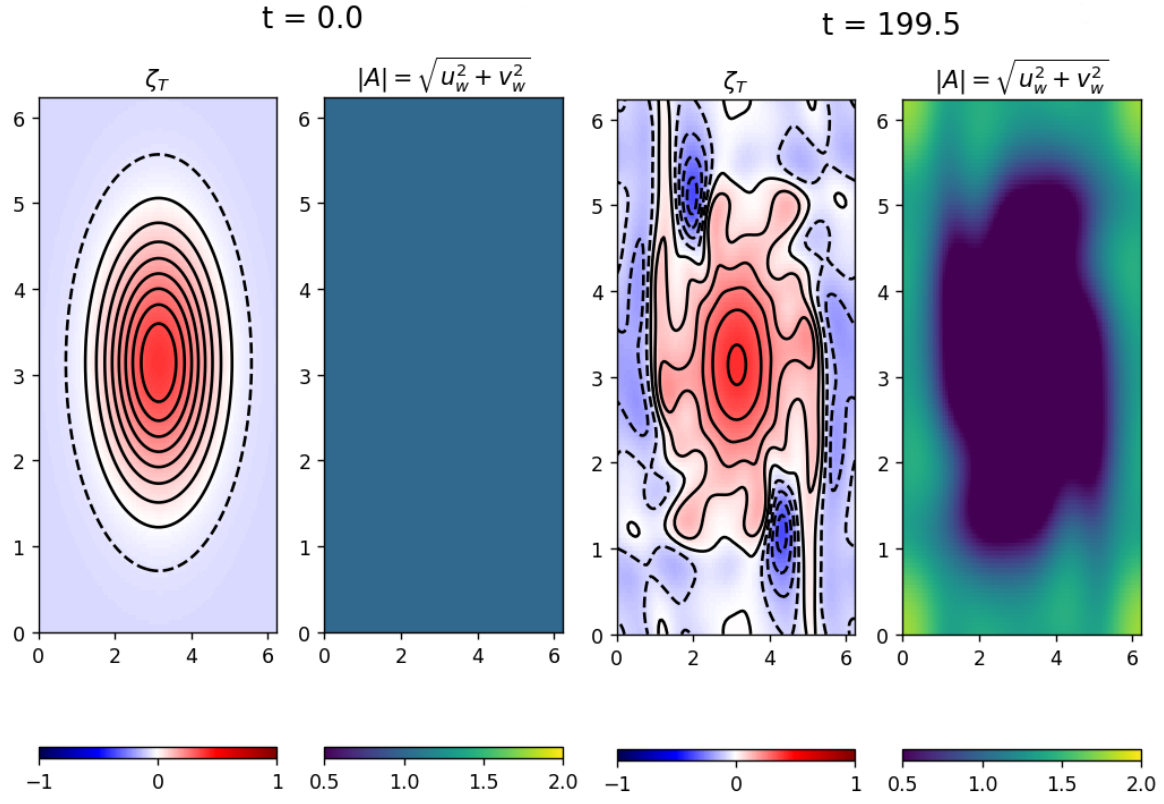


Figure 8: Same as Figure 7 but initialized with a barotropic cyclone.

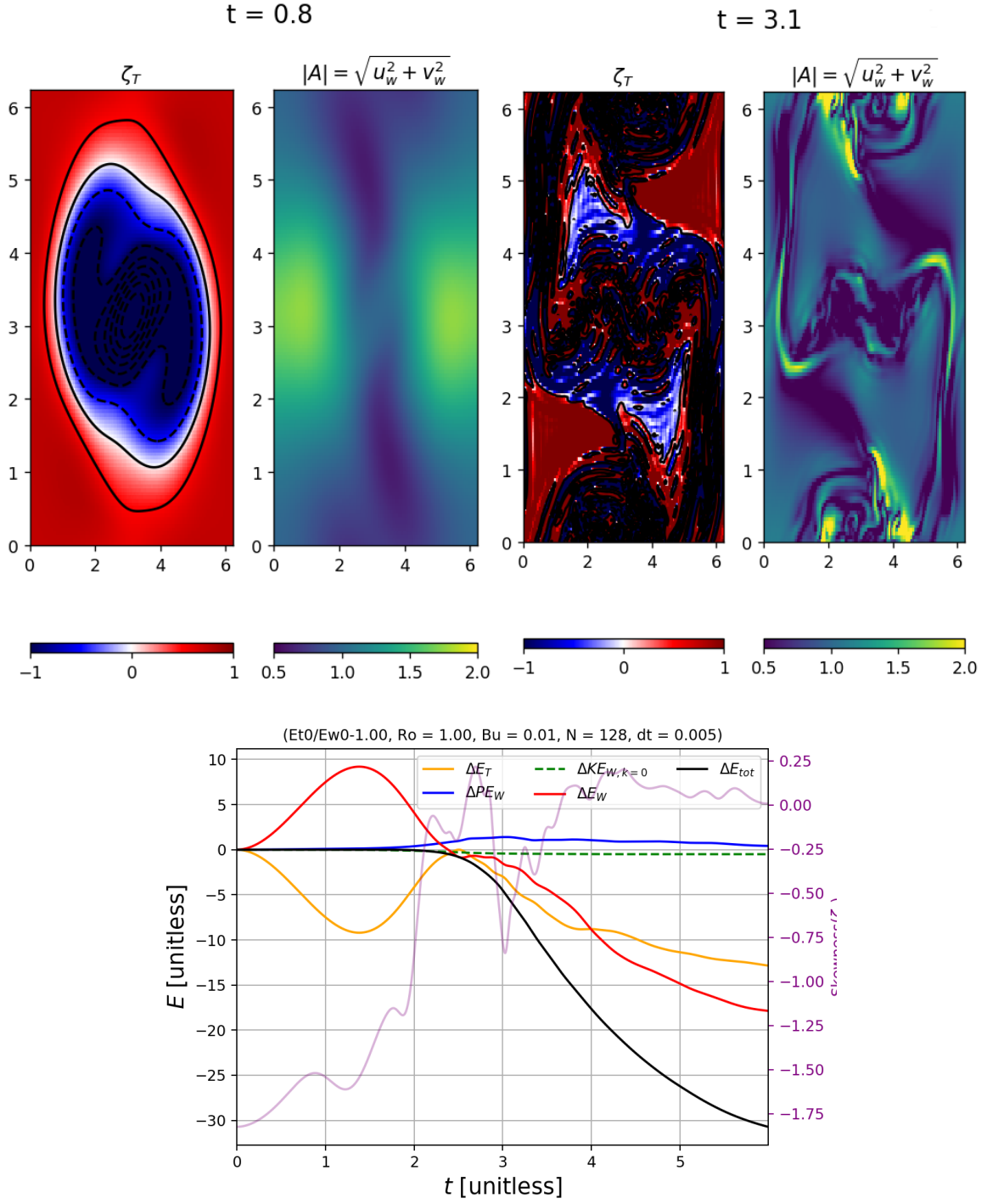


Figure 9: Same as Figure 7, but initialized with a barotropic anticyclone with  $Ro = 1$ .

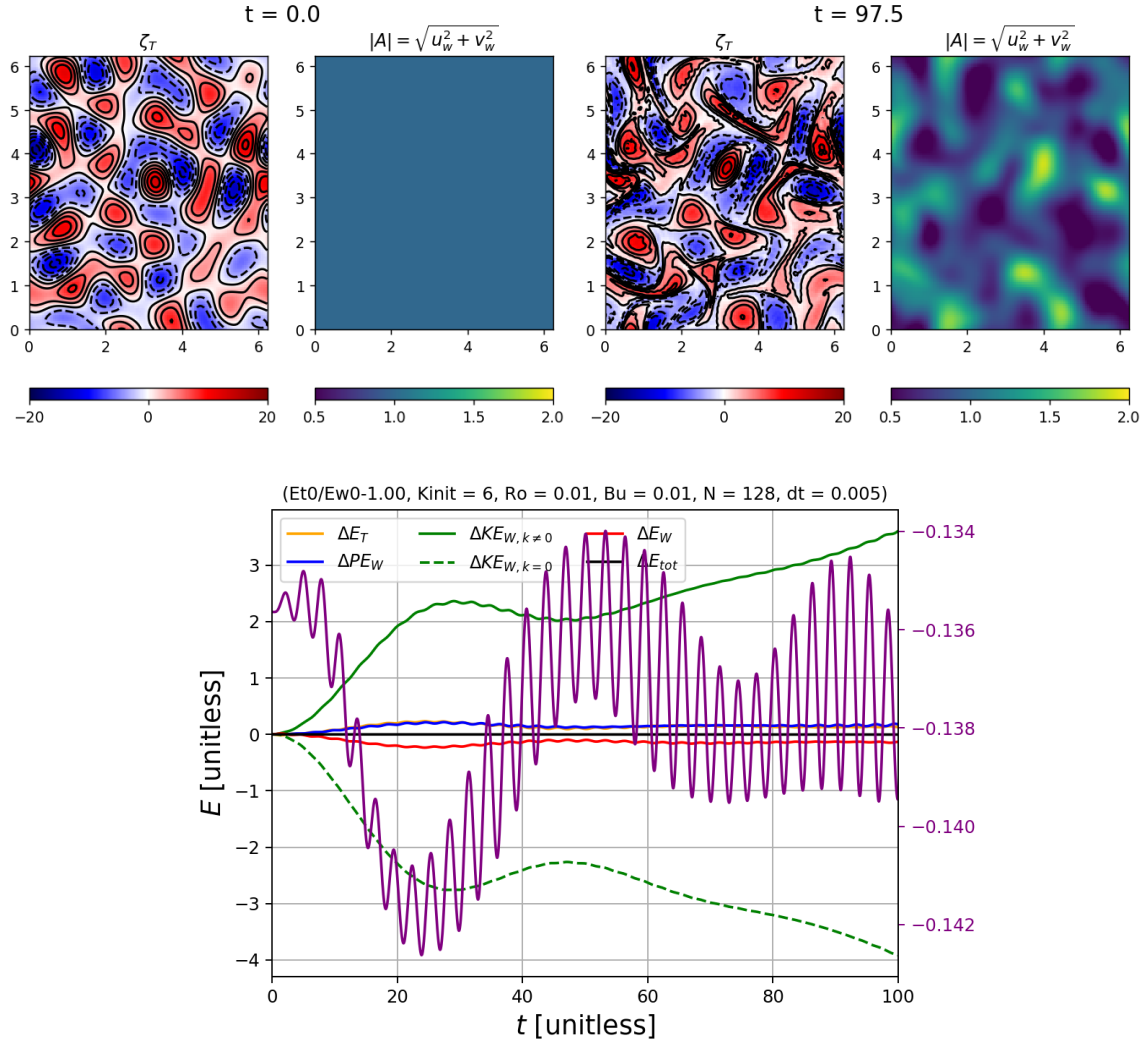


Figure 10: Same as Figure 7, but initialized with 6 wavenumbers with randomized phase and the same initial energy in the balanced and wave modes, *i.e.*,  $E_{t0}/E_{w0} = 1$ .  $Ro = Bu = 0.01$ .

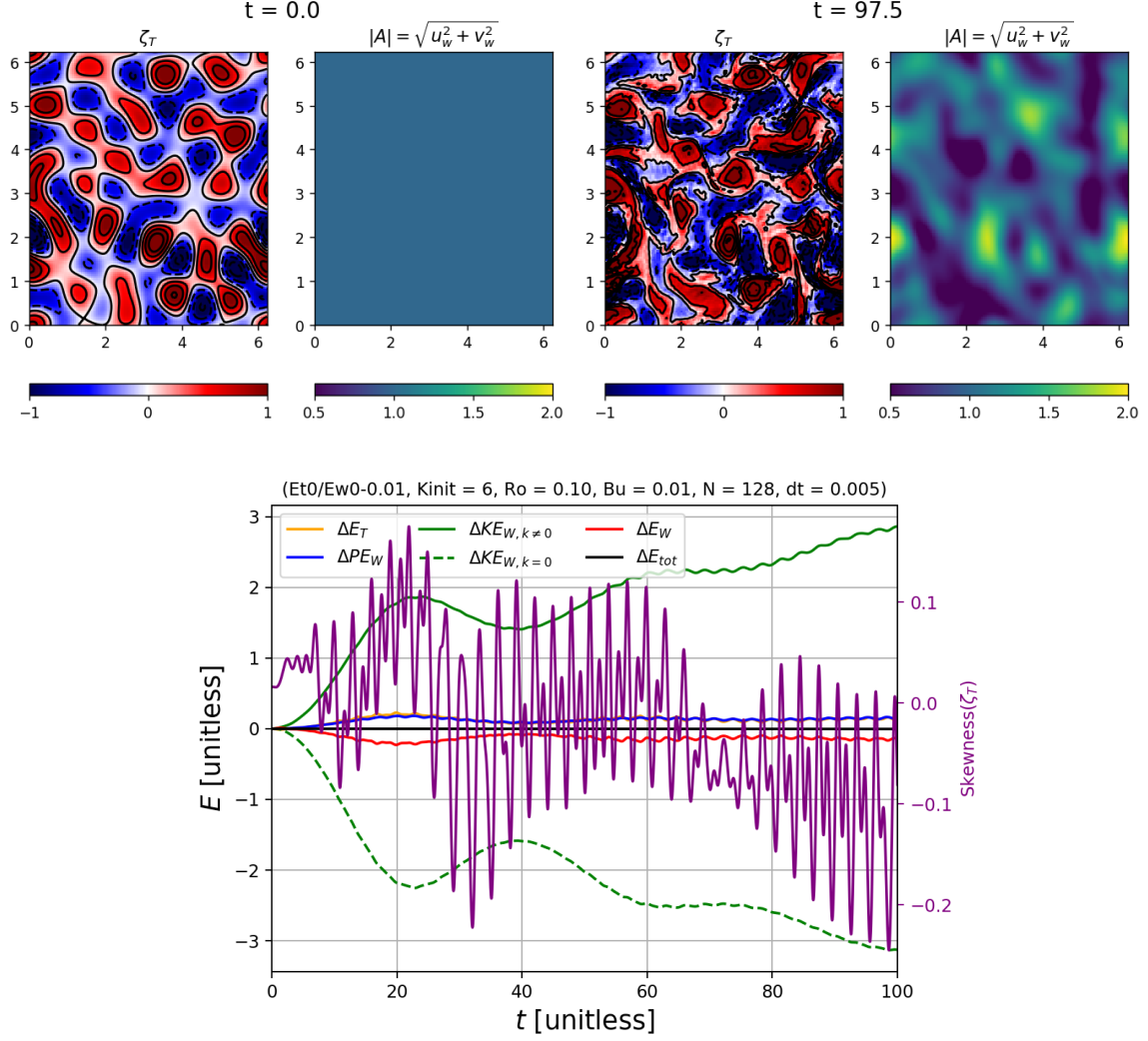


Figure 11: Same as Figure 7, but initialized with 6 wavenumbers with randomized phase, and a hundred times more initial energy in the wave modes, *i.e.*,  $E_{t0}/E_{w0} = 0.01$ .  $Ro = 0.1$  and  $Bu = Ro^2 = 0.01$ ).

## 6 Asymptotic model for NIWs-balanced flow interaction

In this section we derive a new asymptotic model that represents both clockwise and counterclockwise wave modes. We begin with the truncated equations derived by [10], linearized about a steady balanced barotropic flow, written in complex representation:

$$\mathcal{U}_t + i\mathcal{U} + 2\text{Bu}p_{s^*} + \text{Ro}F^u = 0, \quad (72)$$

$$p_t + \mathcal{U}_s + \bar{\mathcal{U}}_{s^*} + \text{Ro}F^p = 0, \quad (73)$$

where

$$F_u \equiv \mathcal{U}_T + U\mathcal{U}_s + \bar{U}\mathcal{U}_{s^*} + \frac{i}{2}(\mathcal{U}\zeta + \bar{\mathcal{U}}\sigma), \quad (74)$$

$$F_p \equiv p_T + U p_s + \bar{U} p_{s^*}, \quad (75)$$

$$\zeta \equiv \triangle\Psi, \sigma \equiv \triangle^\perp\Psi \quad (76)$$

Following [10]'s Appendix B, the governing equations can be rewritten only in terms of velocity in complex representation as

$$\partial_t(\partial_{tt}^2 + 1 - 4\text{Bu}\partial_{ss^*}^2)\mathcal{U} + \text{Ro}R^u = 0 \quad (77)$$

$$\partial_t(\partial_{tt}^2 + 1 - 4\text{Bu}\partial_{ss^*}^2)p + \text{Ro}R^p = 0, \quad (78)$$

where

$$R^u \equiv iF_t^u - F_{tt}^u + i\text{Bu}(F_{ss^*}^u - F_{ss}^u) + i\text{Bu}(\bar{F}_{ss^*}^u - \bar{F}_{s^*s^*}^u) + 2\text{Bu}(F_{s^*t}^p - iF_{s^*}^p) \quad (79)$$

$$R^p \equiv F_{st}^u + \bar{F}_{s^*t}^u + i(F_{s^*}^u - F_s^u) - F_{tt}^p - F^p. \quad (80)$$

We write the solutions as

$$\mathcal{U} = A^- e^{-i\omega t} + A^+ e^{+i\omega t}, \quad (81)$$

$$p = -\frac{i}{\omega}(A_s^- + \bar{A}_{s^*}^+) e^{-i\omega t} + \frac{i}{\omega}(A_s^+ + \bar{A}_{s^*}^-) e^{+i\omega t} \quad (82)$$

Expanding  $\mathcal{U}$  and  $p$  in powers of  $\text{Ro}$ :

$$\mathcal{U} = \mathcal{U}^{(0)} + \text{Ro}\mathcal{U}^{(1)} + \text{Ro}^2\mathcal{U}^{(2)} + \dots \quad (83)$$

and substituting in the momentum equation,

$$i\omega(\mp\omega^2 \pm 1 \mp 4\text{Bu}\partial_{ss^*}^2)A_0^\mp = 0 \quad (84)$$

$$\underbrace{i\omega(\mp\omega^2 \pm 1 \mp 4\text{Bu}\partial_{ss^*}^2)A_1^\mp}_{\equiv \mathcal{M}^\mp} + R_0^\mp = 0 \quad (85)$$

To obtain a single pair of equations for  $A^\mp \equiv A_0^\mp + \text{Ro}A_1^\mp$ , we follow the reconstitution technique as used by *e.g.*, [6, 12, 8]. The first step is to add a small correction to the RHS of the  $O(1)$  equations:

$$\mathcal{M}^\mp A_0^\mp = \text{Ro}\Phi^\mp \quad (86)$$

$$\mathcal{M}^\mp A_1^\mp + R_0^\mp = 0 \quad (87)$$

Take (86) + Ro  $\times$  (87):

$$\text{Ro}\Phi^\mp = -\text{Ro}[\mathcal{M}^\mp A_1^\mp - R_0^\mp] \quad (88)$$

Substitute back in 86:

$$\mathcal{M}^\mp A^\mp + \text{Ro}R_0^\mp = 0 \quad (89)$$

After some manipulations, the coupled equations for  $A^-$  and  $A^+$  become:

$$[\mathcal{L}^\mp - 2\text{Bu}(1+i)\partial_{ss}^2]A_T^\mp = 2\text{Bu}(1+i)(\overline{A^\pm}_{Ts^*s^*} + \beta^\mp) - \mathcal{L}^\mp \alpha^\mp \dots \quad (90)$$

$$\dots \mp \frac{i\omega}{\text{Ro}}(-\omega^2 + 1 - 4\text{Bu}\partial_{ss}^2)A^\mp + DA^\mp, \quad (91)$$

where the hyperviscosity operator  $D \equiv \nu\Delta^{2r}$  has been added and

$$\mathcal{L}^\mp \equiv \{\omega(\omega \pm 1) + i\text{Bu}[\partial_{ss}^2 - \partial_{ss}^2 + \partial_{ss}^2(\bullet) - \partial_{s^*s^*}^2(\bullet)]\}, \quad (92)$$

$$\alpha^\mp \equiv UA_s^\mp + \overline{U}A_{s^*}^\mp + \frac{i}{2}(A^\mp\zeta + \overline{A^\pm}\sigma), \quad (93)$$

$$\beta^\mp \equiv [U(A_{ss}^\mp + \overline{A^\pm}_{ss^*}) + \overline{U}(A_{ss^*}^\mp + \overline{A^\pm}_{s^*s^*})]_{s^*}. \quad (94)$$

in Cartesian coordinates, Equation 90 reads

$$\left[\mathcal{L}^\mp - \frac{1}{2}\text{Bu}(1+i)\Delta\right]A_T^\mp = 2\text{Bu}(1+i)\left(\frac{1}{4}\Delta^\perp \overline{A^\pm}_T + \beta^\mp\right) - \mathcal{L}^\mp \alpha^\mp \dots \quad (95)$$

$$\dots \mp \frac{i\omega}{\text{Ro}}(-\omega^2 + 1 - \text{Bu}\Delta)A^\mp + DA^\mp,$$

and

$$\mathcal{L}^\mp \equiv \omega(\omega \pm 1) + \frac{i}{2}\text{Bu}(\partial_{yy}^2 + i\partial_{xy}^2) + \frac{i}{2}\text{Bu}(\partial_{yy}^2 - i\partial_{xy}^2)(\bullet). \quad (96)$$

If  $\omega = 1$  and Bu,  $A^+ \rightarrow 0$ , the YBJ [14] amplitude equation is recovered for  $A^-$ :

$$\boxed{A_T^- + \mathbf{U} \cdot \nabla A^- + \frac{i}{2}\left(A^-\zeta - \frac{\text{Bu}}{\text{Ro}}\Delta A^-\right) = 0.} \quad (97)$$

## 6.1 Numerical implementation

Our next goal is to solve 95 numerically. Equation 95 can be rewritten as

$$\begin{aligned} \left[ (\omega \pm 1) - \frac{\text{Bu}}{2} \tilde{\Delta} \right] A_T^\mp - \frac{\text{Bu}}{2} (1+i) \Delta^\perp \overline{A_T^\mp} \pm i\omega(-\omega^2 + 1 - \text{Bu}\Delta) A^\mp - D A^\mp = \dots \\ \dots - \mathcal{L}^\mp \alpha^\mp + 2\text{Bu}(1+i)\beta^\mp, \end{aligned} \quad (98)$$

and semi-discretized with a forward-in-time scheme as

$$\begin{aligned} \left[ \omega(\omega \pm 1) - \frac{\text{Bu}}{2} \tilde{\Delta} \right] \frac{A^\mp(n+1) - A^\mp(n)}{\text{Ro}\delta t} - \frac{\text{Bu}}{2} (1+i) \Delta^\perp \frac{\overline{A^\pm(n+1)} - \overline{A^\pm(n)}}{\text{Ro}\delta t} \dots \\ \dots \pm i\omega(-\omega^2 + 1 - \text{Bu}\Delta) A^\mp(n+1) - D A^\mp(n+1) = -\mathcal{L}^\mp \alpha^\mp(n) + 2\text{Bu}(1+i)\beta^\mp \end{aligned} \quad (99)$$

Multiplying through by  $\text{Ro}\delta t$  and rearranging yields:

$$\begin{aligned} \left[ \omega(\omega \pm 1) - \frac{\text{Bu}}{2} \tilde{\Delta} \pm i\omega\text{Ro}\delta t(-\omega^2 + 1 - \text{Bu}\Delta) - \text{Ro}\delta t D \right] A^\mp(n+1) - \frac{\text{Bu}}{2} (1+i) \Delta^\perp \overline{A^\pm(n+1)} = \dots \\ \dots \left[ \underbrace{\omega(\omega \pm 1) - \frac{\text{Bu}}{2} \tilde{\Delta}}_{\equiv \tilde{\mathcal{L}}^\mp} A^\mp(n) - \frac{\text{Bu}}{2} (1+i) \Delta^\perp \overline{A^\pm(n)} + \text{Ro}\delta t (2\text{Bu}(1+i)\beta^\mp(n) - \mathcal{L}^\mp \alpha^\mp(n)) \right] \end{aligned} \quad (100)$$

where

$$\tilde{\Delta} \equiv \partial_{xx}^2 + \partial_{yy}^2 + \partial_{xy}^2 + i\partial_{xx}^2 \quad (101)$$

and the  $(n)$  and  $(n+1)$  superscripts indicate the time step at which the term is evaluated. Writing  $A^\mp$  in terms of their real and imaginary parts, *i.e.*,  $A^\mp = A_R^\mp + iA_I^\mp$ , we have

$$\begin{aligned} \left[ \tilde{\mathcal{L}}^\mp \pm i\omega\text{Ro}\delta t(-\omega^2 + 1 - \text{Bu}\Delta) - \text{Ro}\delta t D \right] (A_R^\mp + iA_I^\mp)^{(n+1)} - \frac{\text{Bu}}{2} (1+i) \Delta^\perp (A_R^\pm - iA_I^\pm)^{(n+1)} = \dots \\ \dots \tilde{\mathcal{L}}^\mp (A_R^\mp + iA_I^\mp)^{(n)} - \frac{\text{Bu}}{2} (1+i) \Delta^\perp (A_R^\pm - iA_I^\pm)^{(n)} + \text{Ro}\delta t (2\text{Bu}(1+i)\beta^\mp(n) - \mathcal{L}^\mp \alpha^\mp(n)) \end{aligned} \quad (102)$$

Equation 102 and its complex conjugate can be written respectively as

$$\mathcal{H}_1^\mp A_R^{\mp(n+1)} + i\mathcal{H}_1^\mp A_I^{\mp(n+1)} + \mathcal{H}_2 A_R^{\pm(n+1)} - i\mathcal{H}_2 A_I^{\pm(n+1)} = R^{\mp(n)} \quad (103)$$

and

$$\overline{\mathcal{H}_1^\mp} A_R^{\mp(n+1)} - i\overline{\mathcal{H}_1^\mp} A_I^{\mp(n+1)} + \overline{\mathcal{H}_2} A_R^{\pm(n+1)} + i\overline{\mathcal{H}_2} A_I^{\pm(n+1)} = \overline{R^{\mp(n)}}. \quad (104)$$

In matrix form,

$$\begin{bmatrix} \mathcal{H}_1^- & i\mathcal{H}_1^- & \mathcal{H}_2 & -i\mathcal{H}_2 \\ \mathcal{H}_2 & -i\mathcal{H}_2 & \mathcal{H}_1^+ & i\mathcal{H}_1^+ \\ \overline{\mathcal{H}_1} & -i\overline{\mathcal{H}_1} & \overline{\mathcal{H}_2} & i\overline{\mathcal{H}_2} \\ \overline{\mathcal{H}_2} & i\overline{\mathcal{H}_2} & \overline{\mathcal{H}_1}^+ & -i\overline{\mathcal{H}_1}^+ \end{bmatrix} \begin{bmatrix} A_R^{-(n+1)} \\ A_I^{-(n+1)} \\ A_R^{+(n+1)} \\ A_I^{+(n+1)} \end{bmatrix} = \begin{bmatrix} R^{-(n)} \\ R^{+(n)} \\ \overline{R^{-(n)}} \\ \overline{R^{+(n)}} \end{bmatrix} \quad (105)$$

The next step is to implement and time-step this system numerically.

## 7 Conclusions

The main results of this project are as follows:

- A new two-component 2D model seems to reproduce the energetics of more complex 3D models, *i.e.*, **energy transfer from NIWs to the balanced flow at low Ro**;
- This might be the simplest non-asymptotic two-component model that also captures **balanced energy dissipation at high Ro**;
- Idealized models such as the ones developed in this study can be used as **testbeds for parameterizations** for global 3D models in regions of high NIW energy (instead of artificially enhanced viscosity) and
- A **new asymptotic model** was derived for NIW-balanced flow interactions.

## 8 Next steps

The next steps in this project are to

- Verify if the **direction of the energy exchange** (NIWs→balanced) changes as  $Ro = O(1)$  is approached (computationally demanding) and
- **Test the new asymptotic model** against the parent T-W model.

## Acknowledgements

It is a pleasure to acknowledge the work of the directors, Claudia Cenedese, Bruce Sutherland and Karl Helfrich, in running a wonderful and inspiring GFD summer. Thanks to the other fellows and the GFD staff, visitors and seminar speakers for stimulating and insightful discussions. Many thanks to Jim Thomas for proposing and patiently supervising this project.

## References

- [1] R. BARKAN, K. B. WINTERS, AND J. C. MCWILLIAMS, *Stimulated Imbalance and the Enhancement of Eddy Kinetic Energy Dissipation by Internal Waves*, J. Phys. Oceanogr., 47 (2017), pp. 181–198.
- [2] S. J. BENAVIDES AND A. ALEXAKIS, *Critical transitions in thin layer turbulence*, J. Fluid Mech., 822 (2017), pp. 364–385.
- [3] R. FERRARI AND C. WUNSCH, *The distribution of eddy kinetic and potential energies in the global ocean*, Tellus A, 62 (2010), pp. 92–108.
- [4] D. M. FRIERSON, A. J. MAJDA, AND O. M. PAULUIS, *Large scale dynamics of precipitation fronts in the tropical atmosphere: A novel relaxation limit*, Commun. Math. Sci., 2 (2004), pp. 591–626.
- [5] M. REMMEL AND L. SMITH, *New intermediate models for rotating shallow water and an investigation of the preference for anticyclones*, J. Fluid. Mech., 635 (2009), pp. 321–359.
- [6] A. ROBERTS, *An introduction to the technique of reconstitution*, SIAM journal on mathematical analysis, 16 (1985), pp. 1243–1257.
- [7] C. B. ROCHA, G. L. WAGNER, AND W. R. YOUNG, *Stimulated generation: extraction of energy from balanced flow by near-inertial waves*, J. Fluid Mech., 847 (2018), pp. 417–451.
- [8] J. THOMAS, *New model for acoustic waves propagating through a vortical flow*, J. Fluid Mech., 823 (2017), pp. 658–674.
- [9] J. THOMAS AND S. ARUN, *Near-inertial waves and geostrophic turbulence*, Phys. Rev. Fluids, 5 (2020), p. 014801.
- [10] J. THOMAS, K. S. SMITH, AND O. BÜHLER, *Near-inertial wave dispersion by geostrophic flows*, J. Fluid. Mech., 817 (2017), p. 406–438.
- [11] J. THOMAS AND R. YAMADA, *Geophysical turbulence dominated by inertia-gravity waves*, J. Fluid Mech., 875 (2019), pp. 71–100.
- [12] G. L. WAGNER AND W. R. YOUNG, *A three-component model for the coupled evolution of near-inertial waves, quasi-geostrophic flow and the near-inertial second harmonic*, J. Fluid Mech., 802 (2016), pp. 806–837.
- [13] J.-H. XIE AND J. VANNESTE, *A generalised-Lagrangian-mean model of the interactions between near-inertial waves and mean flow*, J. Fluid Mech., 774 (2015), pp. 143–169.
- [14] W. R. YOUNG AND M. B. JELLOUL, *Propagation of near-inertial oscillations through a geostrophic flow*, J. Mar. Res., 55 (1997), pp. 735–766.